Journal of Vacuum Science and Technology A

RESEARCH ARTICLE | FEBRUARY 15 2023

Optical studies of pure and (Cu, Co) doped nickel zinc ferrite films deposited on quartz substrate

Sneha Kothapally ; Sushma Kotru ; Roni Paul ; Jaber A. Abu Qahouq

Check for updates

J. Vac. Sci. Technol. A 41, 023404 (2023)
https://doi.org/10.1116/6.0002262

View Online
Export Citation
CrossMark

22 November 2023 16:14:54

JVST A
Journal of Vacuum Science & Technology A

ARTICLE

avs.scitation.org/journal/jva

Optical studies of pure and (Cu, Co) doped nickel zinc ferrite films deposited on quartz substrate

Cite as: J. Vac. Sci. Technol. A **41**, 023404 (2023); doi: 10.1116/6.0002262
Submitted: 7 October 2022 · Accepted: 13 January 2023 ·
Published Online: 15 February 2023

View Online Export Citation CrossMark

Sneha Kothapally, Sushma Kotru,[a] Roni Paul, and Jaber A. Abu Qahouq

AFFILIATIONS

Department of Electrical and Computer Engineering, The University of Alabama, Tuscaloosa, Alabama 35487

[a]**Author to whom correspondence should be addressed:** skotru@eng.ua.edu

ABSTRACT

In this work, the optical properties of pure and doped films were investigated as a function of annealing temperature. Films with compositions $Ni_{0.5}Zn_{0.5}Fe_2O_4$, $Ni_{0.35}Cu_{0.2}Zn_{0.45}Fe_2O_4$, and $Ni_{0.35}Co_{0.2}Zn_{0.45}Fe_2O_4$ were deposited on quartz substrate using the sol–gel method. The grown films were annealed at 500 and 800 °C in a rapid thermal annealing furnace. The single-phase spinel structure of these films was confirmed by x-ray diffraction (XRD) results. The average crystallite size calculated from the XRD data was observed to increase with the annealing temperature and decrease for films doped with Cu and Co. The lattice constant was observed to decrease with the annealing temperature and increase for films doped with Cu and Co. The cross-sectional images obtained from field emission scanning electron microscope were used to calculate the thickness of these films. Ultraviolet-visible spectroscopy was used to obtain the absorbance spectra as a function of wavelength in the range of 200–800 nm. The bandgap obtained from the absorbance spectra was seen to decrease for films annealed at higher temperatures for pure and doped films. Furthermore, the bandgap of doped films was seen to decrease in comparison to that of pure films. Optical parameters such as refractive index, extinction coefficient, optical conductivity, and real and imaginary parts of the dielectric constant were observed to increase with the reduction in the bandgap.

Published under an exclusive license by the AVS. https://doi.org/10.1116/6.0002262

22 November 2023 16:14:54

I. INTRODUCTION

Ferrite materials are used in magnetic applications like multilayer chip inductors,[1] magnetic recording,[2] and power converters[3] due to their low eddy current losses, high resistivity, and high permeability.[4–7] The band structure of certain ferrite materials such as zinc ferrite, nickel ferrite, and nickel zinc ferrite indicates that they can also be used as semiconductors.[8] These materials find applications in energy storage, wastewater treatment, radar absorbing devices, gas sensor, photocatalysts, and radiotherapy.[1–3,9] Recently, the research community has started to explore their use based on optical properties for optical coatings,[10] filters, modulators, and switches[11] and other optoelectronic devices including solar cells as window layers and antireflection coatings.[12] Tuning the optical properties of ferrites for designing the optoelectronic devices is an evolving field.[13]

The bulk form of ferrites is not compatible with modern electronic applications as the trend of miniaturizing electronic components is preferred. This necessitates the fabrication of ferrites in the form of thin films. Various deposition techniques including sputter deposition,[14–16] chemical vapor deposition,[17,18] pulsed laser deposition,[19–21] sol–gel deposition,[11,22,23] and spin–spray deposition[24,25] have been used to fabricate ferrite thin films.

Sun *et al.* studied the structural and magnetic properties of NZF thin films deposited on various substrates [Si(100), Si(111) and $MgAl_2O_4$(100)] by the magnetron sputtering method and his studies indicate that the NZF deposited on $MgAl_2O_4$(100) showed better properties.[26] Wu *et al.* studied NZFO films deposited on the Pt/Ti/SiO_2/Si substrate using radio frequency magnetron sputtering.[27] Desai *et al.* studied the effect of annealing temperature on magnetic properties of $Ni_{0.5}Zn_{0.5}Fe_2O_4$ (NZF) films sputtered on fused quartz and Si substrate.[28] Gupta *et al.* conducted magnetic studies on nanocrystalline nickel zinc ferrite films spin coated on ITO-coated 7059 glass and annealed at a temperature of 650 °C.[29] Rajaram *et al.* studied the magnetic properties of NZF ceramic films prepared by aerojet printing on the Ag/glass substrate for power transfer applications.[30] Kumar *et al.* investigated the effect of Co-doping on saturation magnetization and coercivity of NZF nanoparticles.[31] Xiang *et al.* explained the variation in saturation magnetization and coercivity of NZF with Cu concentration.[32]

Published under an exclusive license by the AVS

Though magnetic properties of ferrites have been vastly investigated, there is not much work on optical studies. Optical measurements such as absorbance, transmittance, and reflectance are based on the electronic transitions that occur in the materials and can be used to determine the optical constants such as refractive index, extinction coefficient, optical conductivity, and dielectric constant. These measurements also provide the necessary parameters to determine the bandgap of the material. Tuning the optical properties such as bandgap is essential for optoelectronic applications which can be achieved by doping. Optical properties are influenced by several factors like microstructure of the film, grain size, lattice parameter, crystallite size, annealing temperature, processing technique, concentration, and doping.[11,33,34] Rao *et al.* studied the structural and optical properties of nanocrystalline (Co, Cu, Ni, Zn) ferrite thin films and reported the bandgap values between 1.7 and 1.9 eV.[35] Pawar *et al.* reported that the bandgap value increased from 2.24 to 2.54 eV with Zn concentration in $Ni_{1-x}Zn_xFe_2O_4$ (NZF) films.[11] Chavan *et al.* studied the effect of zinc concentration on structural and optical properties of nanocrystalline nickel zinc ferrite thin films deposited on a glass substrate by the chemical bath method. His studies indicate that the bandgap increased with Zn concentration which was attributed to change in structure.[36] Alzahrani *et al.* investigated the effect of calcination temperature on optical properties of $(ZnO)_{0.8}$ $(ZrO_2)_{0.2}$ nanoparticles and observed a reduction in bandgap with an increase in temperature.[37] Dixit *et al.* studied the effect of thickness on the structural, magnetic, and optical properties of nickel ferrite thin films deposited by the pulsed laser deposition technique on a silicon substrate and observed that the bandgap (5.7 eV) was independent of the thickness of the film.[38]

In our previous work, the effect of (Cu, Co) doping on the magnetic properties of NZF films deposited on the Si/SiO_2 substrate was investigated.[23] For optical studies, the films need to be deposited on transparent substrates such as quartz to obtain better transmission of light. In this work, we prepared $Ni_{0.5}Zn_{0.5}Fe_2O_4$ (NZF), $Ni_{0.35}Cu_{0.2}Zn_{0.45}Fe_2O_4$ (NCuZF), and $Ni_{0.35}Co_{0.2}Zn_{0.45}Fe_2O_4$ (NCoZF) films on quartz substrates using the sol–gel method and annealed them at two different temperatures (500 and 800 °C). Structural and optical properties of these films were investigated to understand the effect of doping and annealing temperature on these properties. Tunable bandgap and other optical constants can lead to optoelectronic applications. The sol–gel deposition technique was chosen because of its advantages including control over stoichiometry and chemical composition, fabrication of large-area thin films without the need of high vacuum environment, low fabrication cost, and processing temperatures.[39] To the best of our knowledge, the effect of doping (Cu, Co) on optical properties of NZF films has not been reported in the literature.

II. EXPERIMENT

A. Preparation

Detailed explanation about the preparation of solutions and thin films can be found in our previous communication.[23] Here, we have presented a summary of the preparation steps. Three separate solutions (hereafter referred as "sol") of NZF, NCuZF, and NCoZF were prepared using the starting materials $Ni(OCOCH_3)_2{\cdot}4H_2O$, $Zn(CH_3COO)_2{\cdot}2H_2O$, $Fe(NO_3)_3{\cdot}9H_2O$, and $Co(NO_3)_2{\cdot}6H_2O$, $Cu(NO_3)_2{\cdot}3H_2O$. The appropriate amount of corresponding precursors for each solution determined from the desired composition and the molarity were dissolved in the solvent (dimethylformamide) and stirred for 1h. The molarity of each solution was adjusted to 0.5 M by adding acetic acid and stirred for 2 more hours. After stirring, these solutions were kept undisturbed for 36h to form the "sol" for NZF, NCuZF, and NCoZF. These solutions were used to deposit three sets of films, one each for NZF, NCuZF, and NCoZF, on quartz substrates using the spin coating technique. Parameters like rotation speed and spin time of the spinner were optimized to 4000 rpm and 50 s, respectively, to achieve the desired thickness for each layer (~100 nm). The films were hydrolyzed at 120 °C for 30 min to remove the solvent and pyrolyzed at 400 °C for 30 min to exclude any organic substances using hotplate. These steps were repeated three times to achieve the desirable thickness of ~300 nm for NZF, NCuZF, and NCoZF films. One film from each set was left as-deposited (unannealed), and the remaining films were annealed at two different temperatures (500 and 800 °C). A rapid thermal annealing furnace (RTA) was used to anneal the films at 500 and 800 °C in flowing oxygen (2000 SCCM) to promote the crystallinity.

B. Characterization

All films were characterized for structural and optical properties using x-ray diffractometer (XRD) and ultraviolet-visible (UV-Vis) Spectrophotometer. Bruker D8 Discover with Co Kα radiation at 40 kV and 35 mA was used to study the crystal structure and orientation of the films for 2θ ranging from 10° to 90°. XRD data corresponding to the Co-source were converted to equivalent Cu-source data. Structural parameters like crystallite size and lattice constant were determined from the XRD data. Dislocation density was calculated from an average crystallite size. Apreo Field Emission Scanning Electron Microscope (FE-SEM) was used to measure the thickness. Optical properties were investigated using a Shimadzu UV-VIS 1800 spectrophotometer. The absorbance spectra were recorded at room temperature in the wavelength range of 200–800 nm with a step size of 1 nm. Optical parameters like energy bandgap, refractive index, extinction coefficient, optical conductivity, complex dielectric constant, skin depth, and Urbach energy were determined from the absorbance data.

III. RESULTS AND DISCUSSION

A. Structural properties

Figures 1(a)–1(c) show x-ray diffraction pattern of as-deposited and annealed NZF, NCuZF, and NCoZF films. NZF films exhibited (111), (220), (311), (222), (400), (422), (333), and (440) diffraction peaks. NCuZF and NCoZF films exhibited same peaks except that (333) in NZF is being replaced by (511) in these films. These peaks were identified on comparing the data with standard ICDD. No diffraction peaks were obtained from as-deposited films confirming their amorphous nature. Films annealed at 800 °C showed intense, sharp, and narrow XRD peaks. Similar peaks were exhibited by the films annealed at 500 °C with lower intensity and

22 November 2023 16:14:54

Published under an exclusive license by the AVS

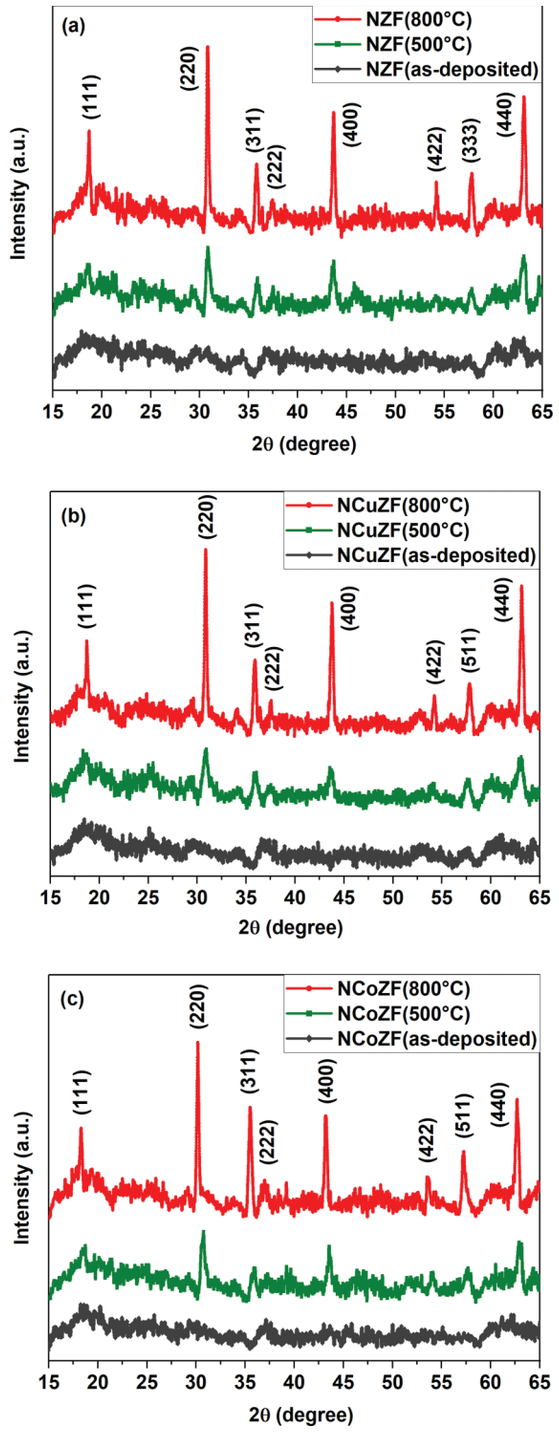

FIG. 1. X-ray diffraction pattern of (a) NZF, (b) NCuZF, and (c) NCoZF films (as-deposited and annealed at 500 and 800 °C).

broader width. These XRD peaks confirm the single-phase spinel structure without any unwanted phases, and the results are in accordance with our previous work.[23]

The lattice constants were calculated from diffraction planes using the following equation:[40]

$$a = d(h^2 + k^2 + l^2)^{\frac{1}{2}}, \tag{1}$$

where a is the lattice constant, d is the interplanar distance, and h, k, and l are the miller indices of the crystal planes. The average crystallite size of these films was obtained by using the Scherrer formula given by[41]

$$D = \frac{0.9\lambda}{\beta \cos\theta}, \tag{2}$$

where D is the crystallite size, λ is the wavelength of the x-ray source, β is the full width at half maximum of the diffraction peak, and θ is the diffraction angle. For these calculations, (220), (400), (333/511), and (440) peaks from the XRD data were used. Further, the dislocation density defined as the length of dislocation lines per unit volume of the crystal was calculated using the inverse relationship given by[42]

$$\delta = \frac{1}{D^2}, \tag{3}$$

where δ is the dislocation density and D is the crystallite size. Dislocation density gives the information about the defects that occurs in the crystal during the growth process.

The lattice constant, average crystallite size, and dislocation density determined using Eqs. (1)–(3) for NZF, NCuZF, and NCoZF films are tabulated in Table I. Films annealed at 800 °C showed improved crystallinity compared to the ones annealed at 500 °C which is attributed to the agglomeration of crystallites with an increase in annealing temperature.[43] The reduction in lattice constant and dislocation density is due to the reduced lattice defects and improved crystallinity, respectively, with an increase in annealing temperature.

The highest value of lattice constant was obtained from the NZF films doped with Co, followed by those doped with Cu. Increase in the lattice constant with doping can be explained in

TABLE I. Structural parameters of NZF, NCuZF, and NCoZF films annealed at 500 and 800 °C, determined from the XRD data.

Sample	Annealing temperature (°C)	Lattice constant (Å)	Average crystallite size (nm)	Dislocation density (10^{15} lines/m^2)
NZF	500	8.269 ± 0.029	16.602 ± 1.392	3.38
NZF	800	8.266 ± 0.023	27.291 ± 0.707	1.27
NCuZF	500	8.291 ± 0.007	13.197 ± 2.013	5.61
NCuZF	800	8.273 ± 0.016	26.080 ± 0.504	1.41
NCoZF	500	8.335 ± 0.037	15.830 ± 0.620	4.33
NCoZF	800	8.328 ± 0.039	26.381 ± 0.203	1.32

22 November 2023 16:14:54

Published under an exclusive license by the AVS

terms of ionic radii of substituted (Co, Cu) and displaced (Ni, Zn) ions.[44] The ionic radii of Cu (0.73 Å) and Co (0.735 Å) are greater than Ni (0.69 Å) but smaller than Zn (0.74 Å).[45] From the composition of $Ni_{0.5}Zn_{0.5}Fe_2O_4$, $Ni_{0.35}Cu_{0.2}Zn_{0.45}Fe_2O_4$, and $Ni_{0.35}Co_{0.2}Zn_{0.45}Fe_2O_4$, it is clear that the presence of more Cu or Co ions would displace Ni ions compared to Zn. As a result, the lattice expands, thereby increasing the lattice constant. The average crystallite size of NZF films was highest, followed by NCoZF and NCuZF films.

B. Surface morphology

A representative cross-sectional FE-SEM image of NCoZF annealed at 800 °C is shown in Fig. 2. The film thickness was determined to be 300 ± 10 nm. The film thickness for all the samples was determined from the corresponding cross-sectional FE-SEM images (all images not included here).

C. Optical properties

Figures 3(a)–3(c) show the optical absorbance spectra as a function of wavelength for NZF, NCuZF, and NCoZF films annealed at 500 and 800 °C. The absorbance is high in the ultraviolet region and low in the visible and near infrared region with absorbance band edges varying in the range 525–550 nm. The optical absorption was seen to increase with an increase in annealing temperature from 500 to 800 °C. This could be attributed to an increase in average crystallite size and reduced defects with the increase in annealing temperature.

The absorption coefficient (α) was calculated from the absorbance (A) and sample thickness (t) using the following equation:[41]

$$\alpha = 2.303^{*}\left(\frac{A}{t}\right). \quad (4)$$

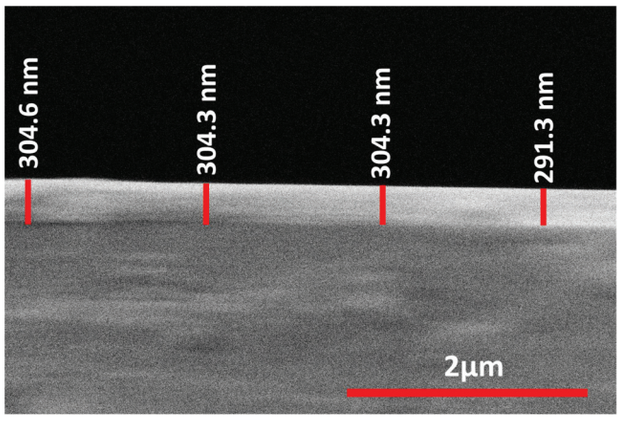

FIG. 2. Cross-sectional FE-SEM image of the NCoZF film annealed at 800 °C.

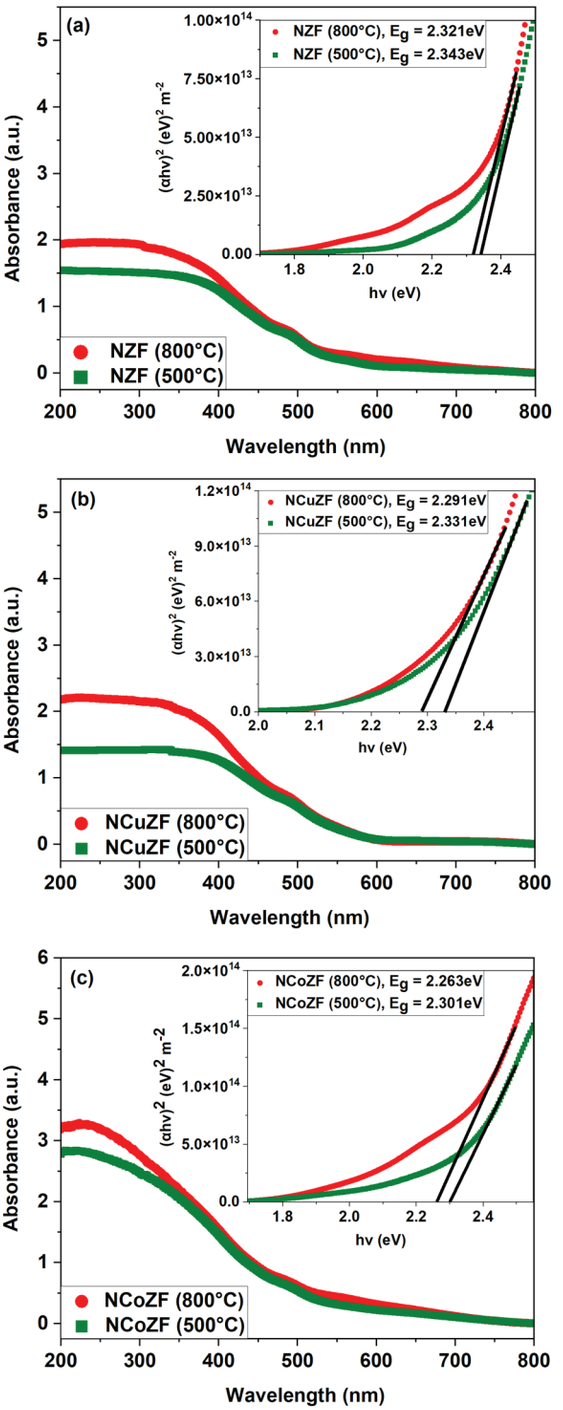

FIG. 3. Absorbance spectra as a function of wavelength (the Tauc plot shown in the inset) for (a) NZF, (b) NCuZF, and (c) NCoZF films annealed at 500 and 800 °C.

22 November 2023 16:14:54

Published under an exclusive license by the AVS

The energy bandgap of these films was determined using the Tauc relation[46] represented by Eq. (5),

$$\alpha h\nu = A\,(h\nu - E_g)^{\frac{1}{n}}, \tag{5}$$

where α is an absorption coefficient determined using Eq. (4), A is a constant which depends on the probability of transition, $h\nu$ is the energy of the incident photon, E_g is an energy bandgap, n is an index having values 2, 1/2, 3, and 3/2 corresponding to allowed direct, allowed indirect, forbidden direct, and forbidden indirect electronic transitions, respectively.[46]

Tauc plots $[(\alpha h\nu)^2$ vs $h\nu]$ for NZF, NCuZF, and NCoZF films annealed at 500 and 800 °C shown as insets of Figs. 3(a)–3(c) are almost linear which confirms the direct bandgap nature of the electronic transitions in these films. The values of direct energy bandgap (E_g) were obtained from these Tauc plots by extrapolating the linear portion of the plot to the energy axis $[(\alpha h\nu)^2 = 0]$ and are presented in Table II. Energy bandgap is influenced by many factors including doping concentration, annealing temperature, crystallite size, lattice parameters, strain, and thickness of the film.[47–49] In addition, redistribution of cations among the tetrahedral and octahedral sites with an increase in annealing temperature has been reported to influence bandgap.[50] From the Tauc plots and Table II, it is seen that the bandgap decreases with an increase in annealing temperature. The reduction in bandgap could be attributed to an increase in average crystallite size and decrease in lattice parameters. It was observed that the bandgap slightly decreased for NZF films doped with Cu and Co, which is attributed to the formation of additional energy sublevels between the valence and conduction bands in the presence of impurities.[51,52]

Refractive index (n) and extinction coefficient (k) which are associated with the amount of light scattered or absorbed by a material can be obtained from the absorbance data using Eqs. (6)–(8),[41,53]

$$n = \frac{1}{T_s} + \frac{1}{(T_s - 1)^{\frac{1}{2}}}, \tag{6}$$

TABLE II. Bandgap and urbach energy values of NZF, NCuZF, and NCoZF films annealed at 500 and 800 °C, determined using the absorbance data.

Sample	Annealing temperature (°C)	Bandgap (E_g) (eV) (±0.01) Tauc plot	Optical dielectric loss plot	Urbach energy (E_U) (eV)
NZF	500	2.343	2.339	0.391 ± 0.024
NZF	800	2.321	2.318	0.471 ± 0.018
NCuZF	500	2.331	2.328	0.354 ± 0.038
NCuZF	800	2.291	2.293	0.316 ± 0.047
NCoZF	500	2.301	2.289	0.507 ± 0.012
NCoZF	800	2.263	2.258	0.547 ± 0.021

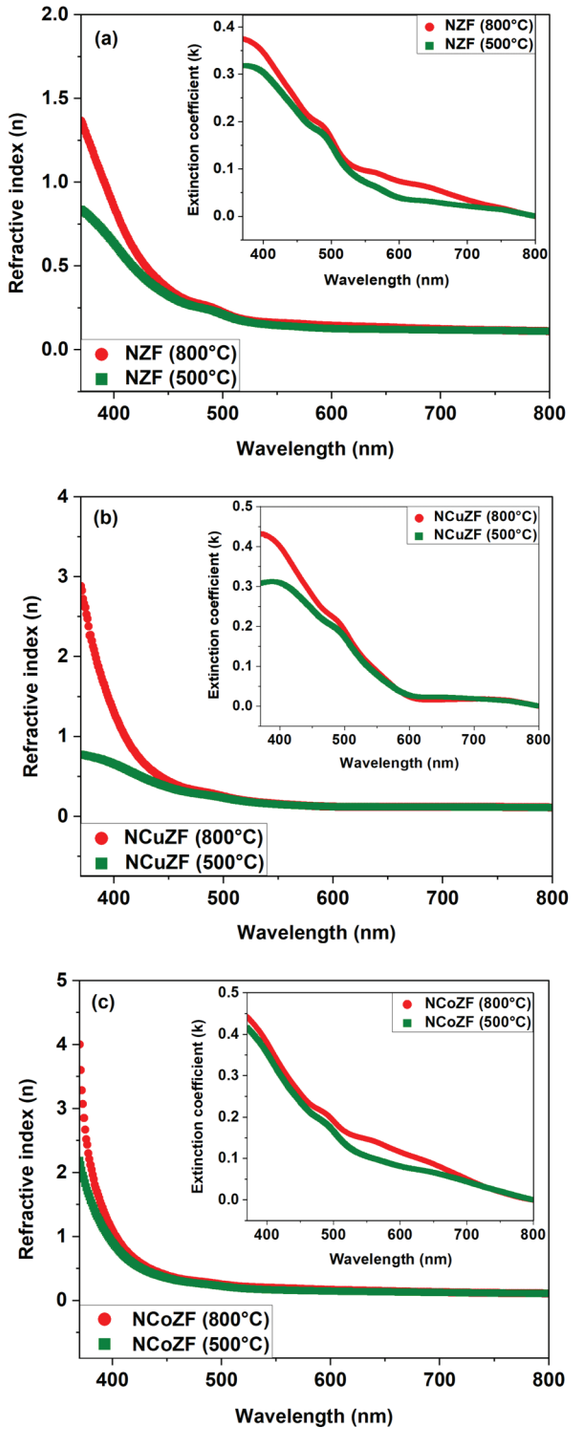

FIG. 4. Refractive index and extinction coefficient as a function of wavelength for (a) NZF, (b) NCuZF, and (c) NCoZF films annealed at 500 and 800 °C.

22 November 2023 16:14:54

Published under an exclusive license by the AVS

$$T_S = 10^{-A} * 100, \tag{7}$$

$$k = \frac{\alpha\lambda}{4\pi}, \tag{8}$$

where A is an absorbance, T_S is the percentage transmission coefficient, α is the absorption coefficient, and λ is the wavelength of incident light.

Refractive indexes of NZF, NCuZF, and NCoZF films annealed at 500 and 800 °C, as a function of wavelength, are shown in Figs. 4(a)–4(c). The corresponding extinction coefficients are presented as the inset of Figs. 4(a)–4(c). Both "n" and "k" were observed to decrease with an increase in the wavelength in the ultraviolet and visible regions (370–530 nm) which is attributed to low absorption and high transmittance due to less scattering of photons in that region. Higher values of "n" and "k" were observed from the films annealed at higher temperature which is attributed to high density and crystallinity of the films at higher temperature. NZF films doped with Cu or Co resulted in improved "n" and "k" compared to the pure ones due to an increase in absorbance and reduction in energy bandgap.

Optical conductivity (σ) which results from the excitation of electrons among the energy levels (valence to conduction bands) on absorption of photons was calculated using the following equation:[41]

$$\sigma = \frac{\alpha n c}{4\pi}, \tag{9}$$

where α is the absorption coefficient, n is the refractive index determined using Eq. (6), and c is the velocity of light.

Figure 5 shows the optical conductivity of NZF, NCuZF, and NCoZF films annealed at 500 and 800 °C, as a function of

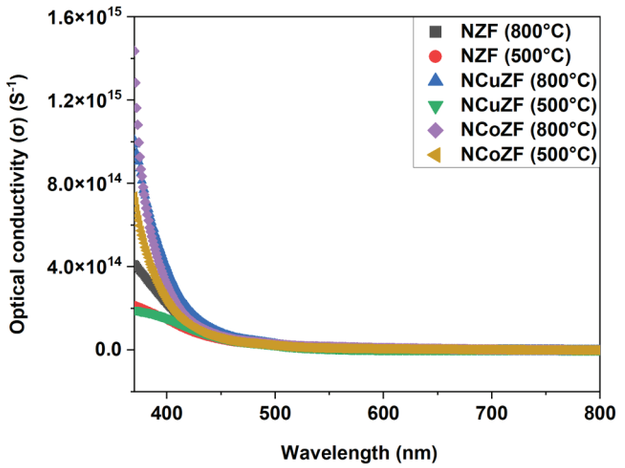

FIG. 5. Optical conductivity as a function of wavelength for NZF, NCuZF, and NCoZF films annealed at 500 and 800 °C.

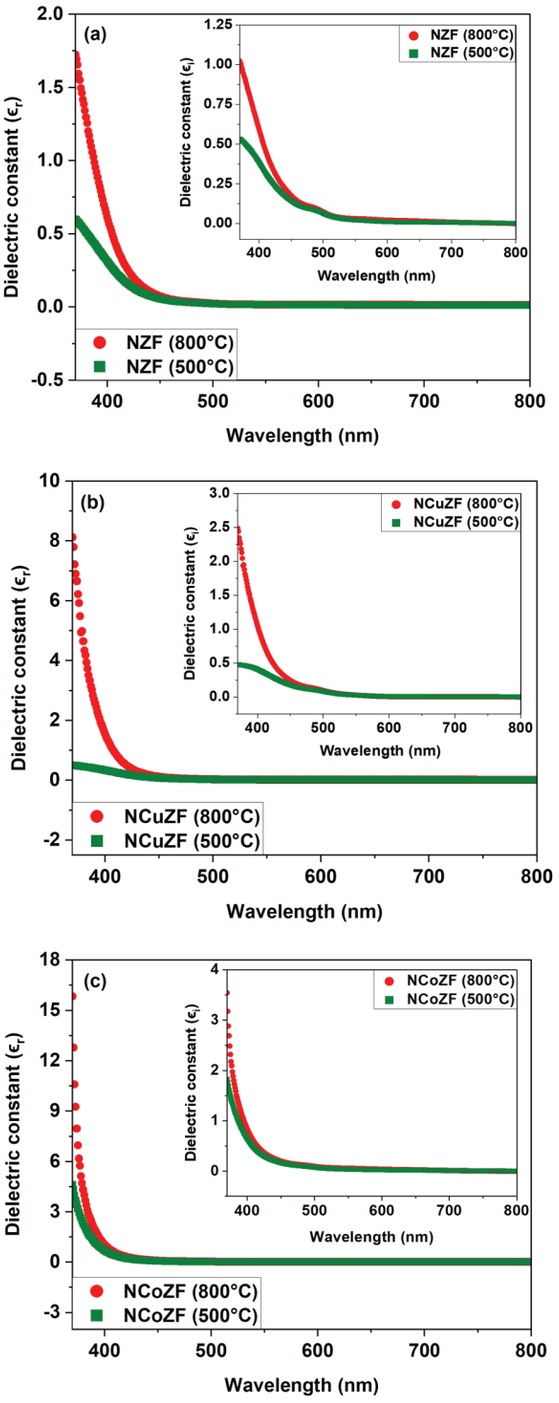

FIG. 6. Real and imaginary parts of dielectric constant as a function of wavelength for (a) NZF, (b) NCuZF, and (c) NCoZF films annealed at 500 and 800 °C.

22 November 2023 16:14:54

Published under an exclusive license by the AVS

wavelength. The optical conductivity was observed to decrease with an increase in wavelength due to the reduction in absorbance and refractive index, as predicted by Eq. (9). Higher annealing temperatures and doping improved optical conductivity due to the reduction in bandgap and high absorbance.

Complex dielectric constant (ε) was determined from Eq. (10),[41]

$$\varepsilon = \varepsilon_r + \varepsilon_i = (n^2 - k^2) + i\,(2nk), \tag{10}$$

where ε_r is the real part of dielectric constant and ε_i is the imaginary part which is associated with the absorption of radiation by free carrier, n is the refractive index, and k is the extinction coefficient.

Figures 6(a)–6(c) show the real part of dielectric constant "ε_r" of NZF, NCuZF, and NCoZF films annealed at 500 and 800 °C, as a function of wavelength and the imaginary part "ε_i" as an inset. Both "ε_r" and "ε_i" were observed to decrease with an increase in wavelength and increase with an increase in annealing temperature and doping which agrees with the trend followed by "n" and "k." The values of the optical constants (n, k, ε_i, ε_r, *and* σ) corresponding to the wavelength 370 nm for NZF, NCuZF, and NCoZF films annealed at 500 and 800 °C are summarized in Table III. As it is clear from these data, with the decrease in bandgap, the refractive index, extinction coefficient, optical conductivity, and dielectric constant increased. The increase in these constants was more prominent for both Cu and Co doped NZF films annealed at 800 °C. However, for films annealed at 500 °C, doping of Cu did not show any major variation in the optical constants in comparison to pure NZF films.

Optical dielectric loss parameter (ε_i), which is directly related to the electron transitions from valence band to conduction band,[54] was used to calculate the optical bandgap values and compared to the values obtained from the Tauc plot. The variation in optical dielectric loss parameter ($\varepsilon_i = 2nk$) with respect to energy of the photon ($h\nu$) is considered to study the bandgap. Figures 7(a)–7(c) show the variation of optical dielectric loss as a function of photon energy for pure and doped NZF thin films annealed at 500 and 800 °C. The values of energy bandgap (E_g) were obtained from these plots by extrapolating the linear portion of the plot to the energy axis ($\varepsilon_i = 0$) and are presented in Table II. The energy bandgap values obtained from the Tauc, and optical dielectric loss plots match closely.

The skin depth (SD) is a measure of the distance that an optical beam penetrates through the sample before it is scattered and is calculated using Eq. (11),[55]

$$SD = \frac{\lambda}{2\pi k} = \frac{2}{\alpha}, \tag{11}$$

where k is the extinction coefficient, α is the absorption coefficient, and λ is the wavelength of the light.

Figure 8 shows the variation of skin depth as a function of wavelength for NZF, NCuZF, and NCoZF films annealed at 500 and 800 °C. From the figure, it is observed that above ~540 nm, the skin depth increases with an increase in the wavelength which is attributed to decrease in absorption coefficient and increase in scattering in that region. At 540 nm (referred to as cut-off wavelength), skin depth starts reducing to zero. The corresponding energy is known as the cut-off energy (~2.296 eV in this case). Further, for NZF and NCoZF films, skin depth was observed to decrease with an increase in annealing temperature, which is attributed to an increase in their absorbance with annealing temperature. However, for Cu doped films, skin depth was observed to increase with an increase in annealing temperature, this trend being opposite to what was observed in other two films. NCoZF, which exhibited maximum absorbance, was observed to have low skin depth followed by NZF and NCuZF.

Urbach energy gives information about the defects or disorders and low crystallinity in materials.[56] The Urbach energy relation describes the width of band tails resultant of the exponential rise in the absorption coefficients due to the presence of localized states in the bandgap and is given by Eq. (12),[57]

$$\ln(\alpha) = \ln(\alpha_o) + \frac{h\nu}{E_U}, \tag{12}$$

where α is the absorption coefficient, α_o is the constant, $h\nu$ is the energy of an incident photon, and E_U is the Urbach energy. The Urbach energy is obtained by calculating the inverse of slope from the plot ln (α) vs $h\nu$.

As seen from Table II, urbach energy was observed to increase on doping NZF with Co which is attributed to the presence of localized states between the valence and conduction bands resulting in the reduction of the bandgap. This trend was observed to be opposite on doping with Cu. For NCuZF films, the urbach energy was observed to decrease with an increase in annealing temperature

22 November 2023 16:14:54

TABLE III. Summary of optical constants corresponding to the wavelength 370 nm for NZF, NCuZF, and NCoZF films annealed at 500 and 800 °C.

Sample	Annealing temperature (°C)	Refractive index (n) (±0.01)	Extinction coefficient (k) (±0.01)	Optical conductivity (σ) (S^{-1}) × 10^{14} (±0.01)	Dielectric constant (±0.01)	
					(ε_r)	(ε_i)
NZF	500	0.839	0.317	2.16	0.575	0.53
NZF	800	1.365	0.377	4.16	1.73	1.025
NCuZF	500	0.800	0.312	2.00	0.582	0.501
NCuZF	800	2.884	0.432	10.09	8.163	2.498
NCoZF	500	2.198	0.415	7.43	4.64	1.828
NCoZF	800	4.018	0.445	14.38	15.87	3.565

Published under an exclusive license by the AVS

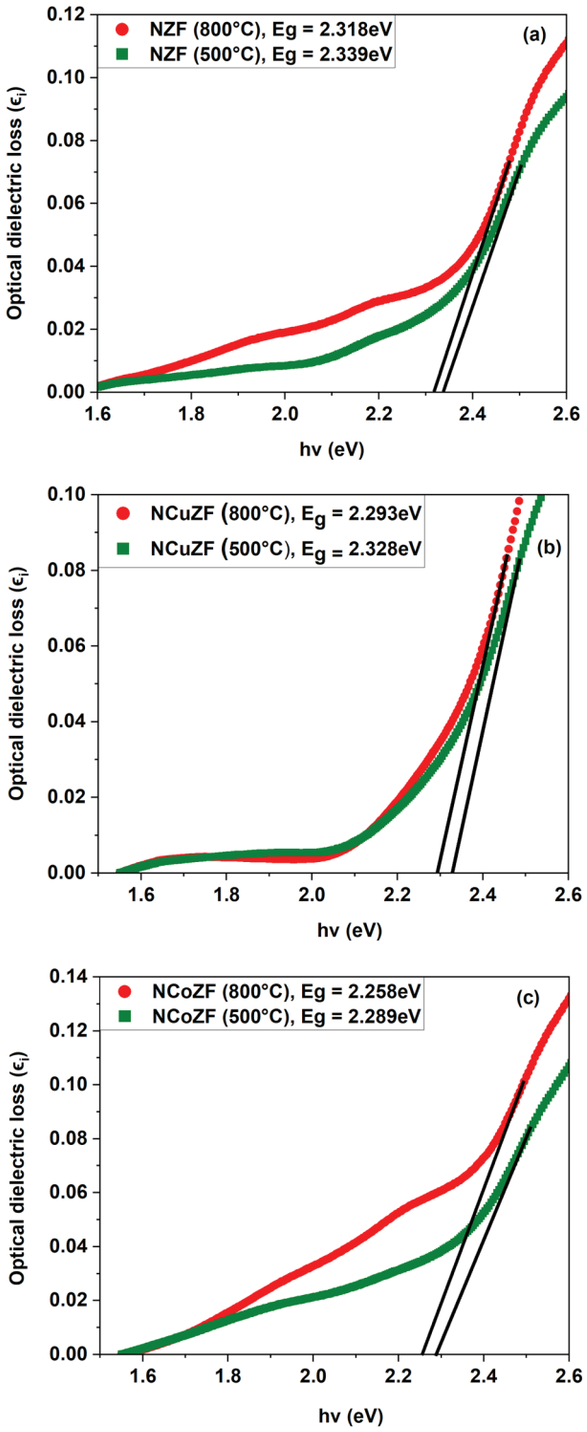

FIG. 7. Optical dielectric loss as a function of photon energy for (a) NZF, (b) NCuZF, and (c) NCoZF films annealed at 500 and 800 °C.

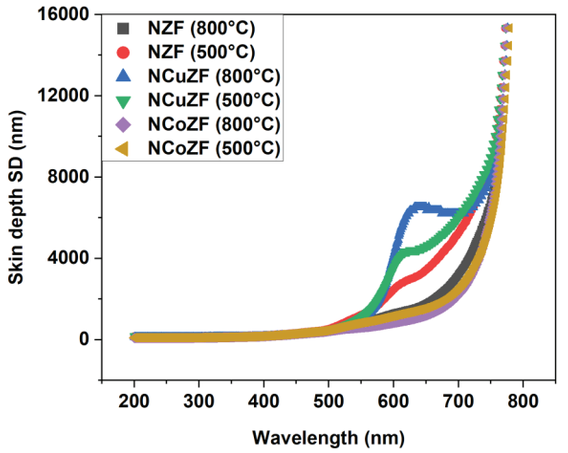

FIG. 8. Skin depth as a function of wavelength for NZF, NCuZF, and NCoZF films annealed at 500 and 800 °C.

due to reduced defects or disorders in the crystal structure due to annealing at higher temperature, whereas the urbach energy was observed to increase with the annealing temperature in the case of pure and Co doped NZF films.

IV. SUMMARY AND CONCLUSIONS

NZF, NCuZF, and NCoZF films were successfully deposited on the quartz substrate using the sol–gel technique. All films were annealed at 500 and 800 °C and used to study the structural and optical properties to understand how these properties vary with the change in annealing temperature. The lattice constant for pure and doped films was observed to decrease with an increase in annealing temperature but increase on doping, the change being from 8.269 to 8.328 Å. Pure NZF films annealed at 800 °C exhibit largest value of average crystallite size (27.291 nm) followed by films doped with Co (26.381 nm) and Cu (26.080 nm) films. A reduction in bandgap (2.343–2.263 eV) with an enhancement in optical constants such as refractive index (0.839–4.018), extinction coefficient (0.317–0.445), optical conductivity (2.16×10^{14}–14.38×10^{14} s^{-1}), and real dielectric constant (0.575–15.87) was observed with doping and annealing temperature. Films doped with Co and annealed at 800 °C showed the lowest bandgap and higher optical constants, followed by films doped with Cu and the pure NZF films. The bandgap values obtained from the Tauc plot are in close agreement with those values obtained from dielectric loss parameter. The variations in skin depth and urbach energy were studied with respect to annealing temperature and doping. In conclusion, it was observed that the bandgap of these films can be tuned by doping and annealing. A tunable bandgap with improved optical constants makes these films a good candidate for optoelectronic applications.

ACKNOWLEDGMENTS

The authors would like to acknowledge National Science Foundation as this work was supported by the National Science

22 November 2023 16:14:54

Foundation under Grant No. 1708690. Any opinions, findings, and conclusions or recommendations expressed in this work are those of the author(s) and do not necessarily reflect the views of the National Science Foundation. This work utilized resources owned and maintained by the Alabama Analytical Research Facility, which is supported by the University of Alabama. The authors also acknowledge the EDGE Labs at the University of Alabama for the characterization facilities.

AUTHOR DECLARATIONS

Conflict of Interest

The authors have no conflicts to disclose.

Author Contributions

Sneha Kothapally: Conceptualization (equal); Data curation (equal); Formal analysis (equal); Investigation (equal); Validation (equal); Visualization (equal); Writing – original draft (equal); Writing – review & editing (equal). **Sushma Kotru:** Conceptualization (equal); Data curation (equal); Formal analysis (equal); Funding acquisition (equal); Project administration (equal); Resources (equal); Supervision (lead); Validation (equal); Visualization (equal); Writing – original draft (equal); Writing – review & editing (lead). **Roni Paul:** Conceptualization (equal); Data curation (equal); Formal analysis (equal); Investigation (equal); Validation (equal); Visualization (equal); Writing – original draft (equal); Writing – review & editing (equal). **Jaber A. Abu Qahouq:** Formal analysis (supporting); Funding acquisition (lead); Project administration (equal); Resources (equal); Supervision (equal); Writing – review & editing (supporting).

DATA AVAILABILITY

The data that support the findings of this study are available from the corresponding author upon reasonable request.

REFERENCES

[1]G. Rana, P. Dhiman, A. Kumar, D. V. N. Vo, G. Sharma, S. Sharma, and M. Naushad, Chem. Eng. Res. Des. **175**, 182 (2021).
[2]Rachna, N. B. Singh, and A. Agarwal, Mater. Today Proc. **5**, 9148 (2018).
[3]D. H. Bang and J. Y. Park, IEEE Trans. Magn. **45**, 2762 (2009).
[4]S. Zahi, J. Electromagn. Anal. Appl. **02**, 56 (2010).
[5]A. Goldman, *Modern Ferrite Technology* (Springer Science & Business Media, New York, 2006).
[6]Z. Zheng, Y. Li, T. Liu, and Q. Feng, IEEE. Trans. Magn. **54**, 2801404 (2018).
[7]P. Thakur, D. Chahar, S. Taneja, N. Bhalla, and A. Thakur, Ceram. Int. **46**, 15740 (2020).
[8]S. Arcaro and J. Venturini *Modern Ferrites in Engineering*, edited by C. P. Bergmann (Springer, New York, 2021).
[9]J. Qiu, C. Wang, and M. Gu, Mater. Sci. Eng. B **112**, 1 (2004).
[10]N. Goswami, S. Surendra, and S. C. Katyal, J. Laser Opt. Photonics **04**, 2 (2017).
[11]C. S. Pawar, M. P. Gujar, and V. L. Mathe, J. Supercond. Novel Magn. **30**, 615 (2017).
[12]A. A. Ibiyemi, O. Akinrinola, and G. T. Yusuf, Appl. Phys. A **128**, 792 (2022).
[13]V. L. S. Vatsalya, G. S. Sundari, Ch. S. L. N. Sridhar, I. L. Prasanna, and Ch. S. Lakshmi, J. Lumin. **252**, 119314 (2022).
[14]D. Guo, X. Fan, G. Chai, C. Jiang, X. Li, and D. Xue, Appl. Surf. Sci. **256**, 2319 (2010).
[15]Y. Liu, Y. Li, H. Zhang, D. Chen, and C. Mu, J. Appl. Phys. **109**, 07A511 (2011).
[16]R. Xu, L. S. Wang, X. L. Liu, M. Lei, H. Z. Guo, Y. Chen, J. B. Wang, and D. L. Peng, J. Alloys Compd. **604**, 43 (2014).
[17]N. Pachauri, B. Khodadadi, A. V. Singh, J. B. Mohammadi, R. L. Martens, P. R. Leclair, C. Mewes, T. Mewes, and A. Gupta, J. Magn. Magn. Mater. **417**, 137 (2016).
[18]N. Li, S. Schafer, R. Datta, T. Mewes, T. M. Klein, and A. Gupta, Appl. Phys. Lett. **101**, 132409 (2012).
[19]D. Ravinder, K. V. Kumar, and A. V. R. Reddy, Mater. Lett. **57**, 4162 (2003).
[20]Y. Liu *et al.*, Mater. Res. Bull. **138**, 111214 (2021).
[21]S. Rajarathinam, U. Ganguly, and N. Venkataramani, Ceram. Int. **48**, 7876 (2022).
[22]Y. Yusuf, R. S. Azis, S. Kanagesan, and G. Bahmanrokh, J. Aust. Ceram. Soc. **53**, 767 (2017).
[23]S. Kotru, R. Paul, and J. A. Abu Qahouq, Mater. Chem. Phys. **276**, 125357 (2022).
[24]H. Liu, Z. Yu, B. Fu, M. Ran, C. Wu, X. Jiang, R. Guo, Z. Lan, and K. Sun, Ceram. Int. **47**, 1318 (2021).
[25]L. Chao, A. Sharma, M. N. Afsar, O. Obi, Z. Zhou, and N. Sun, IEEE Trans. Magn. **48**, 4085 (2012).
[26]K. Sun, Y. Dai, Y. Yang, Z. Yu, H. Liu, X. Jiang, and Z. Lan, Ceram. Int. **42**, 3028 (2016).
[27]L. Wu, C. Dong, X. Wang, J. Li, and M. Li, J. Alloys Compd. **779**, 794 (2019).
[28]M. Desai *et al.*, J. Appl. Phys. **91**, 7592 (2002).
[29]N. Gupta, A. Verma, S. C. Kashyap, and D. C. Dube, J. Magn. Magn. Mater. **308**, 137 (2007).
[30]K. Rajaram and J. Kim, Nano Energy **57**, 317 (2019).
[31]R. Kumar, H. Kumar, R. R. Singh, and P. B. Barman, J. Sol-Gel Sci. Technol. **78**, 566 (2016).
[32]J. Xiang, X. Shen, F. Song, and M. Liu, J. Solid State Chem. **183**, 1239 (2010).
[33]H. J. Kardile, S. B. Somvanshi, A. R. Chavan, A. A. Pandit, and K. M. Jadhav, Optik **207**, 164462 (2020).
[34]A. R. Chavan, R. R. Chilwar, P. B. Kharat, and K. M. Jadhav, J. Supercond. Novel Magn. **31**, 2949 (2018).
[35]P. Rao, R. V. Godbole, D. M. Phase, R. C. Chikate, and S. Bhagwat, Mater. Chem. Phys. **149–150**, 333 (2015).
[36]S. M. Chavan, M. K. Babrekar, S. S. More, and K. M. Jadhav, J. Alloys Compd. **507**, 21 (2010).
[37]J. S. Alzahrani, I. H. Midala, H. M. Kamari, N. M. Al-Hada, C. K. Tim, N. N. S. Nidzam, Z. A. Alrowaili, and M. S. Al-Buriahi, J. Inorg. Organomet. Polym. Mater. **32**, 1755 (2022).
[38]G. Dixit, J. P. Singh, R. C. Srivastava, H. M. Agrawal, and R. J. Chaudhary, Adv. Mater. Lett. **3**, 21 (2012).
[39]Sajjadi and S. Pooyan, J. Polym. Eng. Tech. **13**, 38 (2005).
[40]A. Sutka, S. Lagzdina, G. Mezinskis, A. Pludons, I. Vitina, and L. Timma, IOP Conf. Ser. Mater. Sci. Eng. **25**, 012019 (2011).
[41]S. Yasmeen, F. Iqbal, T. Munawar, M. A. Nawaz, M. Asghar, and A. Hussain, Ceram. Int. **45**, 17859 (2019).
[42]S. Chander and M. S. Dhaka, Physica E **80**, 62 (2016).
[43]M. K. Manglam, S. Kumari, J. Mallick, and M. Kar, Appl. Phys. A **127**, 138 (2021).
[44]G. S. V. R. K. Choudary, P. Prameela, M. C. Varma, A. M. Kumar, and K. H. Rao, Indian J. Mater. Sci. **2013**, 1 (2013).
[45]R. D. Shannon and C. T. Prewitt, Acta Crystallogr. Sect. B **25**, 925 (1969).
[46]J. Tauc *Amorphous and Liquid Semiconductors*, edited by J. Tauc (Springer Science & Business Media, New York, 1974).
[47]S. Joshi, M. Kumar, S. Chhoker, G. Srivastava, M. Jewariya, and V. N. Singh, J. Mol. Struct. **1076**, 55 (2014).
[48]R. B. Kale and C. D. Lokhande, Appl. Surf. Sci. **223**, 343 (2004).
[49]M. A. Humayun, M. A. Rashid, F. A. Malek, and A. N. Hussain, J. Russ. Laser Res. **33**, 387 (2012).

22 November 2023 16:14:54

Published under an exclusive license by the AVS

[50]D. Sharma and N. Khare, Appl. Phys. Lett. **105**, 032404 (2014).
[51]M. Zulqarnain, S. S. Ali, U. Hira, J. F. Feng, M. I. Khan, M. Rizwan, K. Javed, G. Farid, and M. S. Hasan, J. Alloys Compd. **894**, 162431 (2022).
[52]A. Sharma, K. M. Batoo, O. M. Aldossary, S. Jindal, N. Aggarwal, and G. Kumar, J. Mater. Sci. Mater. Electron. **32**, 313 (2021).
[53]K. V. Kumar, Adv. Mater. Phys. Chem. **12**, 33 (2022).
[54]S. B. Aziz, Nanomaterials **7**, 444 (2017).
[55]V. Dalouji and N. Rahimi, Europhys. Lett. **139**, 45002 (2022).
[56]H. Khmissi, S. A. Mahmoud, and A. A. Akl, Optik **227**, 165979 (2021).
[57]A. S. Abouhaswa and T. A. Taha, Polym. Bull. **77**, 6005 (2020).

22 November 2023 16:14:54

Published under an exclusive license by the AVS